Engineering Structures 306 (2024) 117712

Contents lists available at ScienceDirect

Engineering Structures

journal homepage: www.elsevier.com/locate/engstruct

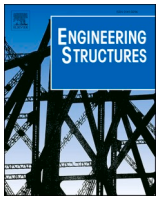

# Robustness assessment of half-joint RC girder bridges

Paolo Martinelli [*,1], Matteo Colombo [2], Marco di Prisco [3]

*Politecnico di Milano, Department of Civil and Environmental Engineering, P.za L. da Vinci 32, 20133 Milan, Italy*

ARTICLE INFO

*Keywords:*
Progressive collapse
Structural robustness
Accidental actions
Beam bridge
Half-joint

ABSTRACT

Considerable research efforts have been dedicated to understanding the resistance of buildings against progressive collapse. However, these efforts have been relatively limited in the context of bridges, despite the equal, if not more, critical importance of robustness criteria in bridge engineering. In the context of existing bridges, it is crucial not only to assess safety, but also to evaluate robustness using reliable metrics. These metrics can aid managing authorities in prioritizing necessary interventions. Considering this, the paper applies various robustness measures to a specific type of reinforced concrete (RC) girder bridge known as half-joint bridges. As a case study, the Annone viaduct is examined, which collapsed in 2016 due to the passage of a heavy truck. A notional removal approach of critical elements to quantify structural robustness is proposed. This approach considers several load configurations, some envisioned during the design stage, and others representing abnormal loads. The study results reveal specific scenarios that may lead to potential progressive collapse and highlight the preferred metrics for this type of bridges. Ultimately, the assessment of robustness can play a key role in choosing a retrofitting solution over other intervention options for existing bridges.

## 1. Introduction

Over the past decade, there has been significant research dedicated to assessing progressive collapse resistance and enhancing structural robustness, primarily in the context of reinforced concrete (RC) frame buildings. However, when it comes to bridges, research efforts in this area have been comparatively limited, even though robustness considerations are equally, if not more, crucial than in building structures. Existing studies on bridge robustness address it both qualitatively and quantitatively, including specific case studies [1–16]. Design strategies to enhance the robustness of bridges con be found in Refs. [3,17]. Literature offers various studies quantifying bridge robustness through both deterministic and probabilistic approaches, some of which are collected in the forthcoming JRC technical report [18]. Regarding deterministic approaches for quantifying the robustness, Wisniewski et al. [12] examined a four-span continuous RC bridge, Cavaco [5] investigated two RC footbridges exposed to corrosion, and Moreira et al. [19] considered a masonry arch railway bridge. In their research, Caredda et al. [16] assessed the robustness of a steel truss-type bridge by exploring different damage scenarios, involving non-simultaneous failures in various elements. Regarding probabilistic robustness measures, notable work includes Biondini and Frangopol [20], who assessed the life-cycle robustness of an RC bridge pier with a box cross-section, and Björnsson and Thelandersson [21], who explored the structural robustness of a multi-span post-tensioned RC bridge in the event of a train collision caused by derailment.

The alarming sequence of bridge collapses in Italy over recent years has underscored the pressing demand for the global evaluation and maintenance of infrastructure assets, primarily comprising RC and precast concrete structures. Evaluating the safety and robustness of existing bridges holds equal significance. The assessment of their robustness can be facilitated using reliable metrics, aiding managing authorities in prioritizing necessary interventions. This paper, within this framework, applies various established robustness measures from the existing literature to a specific type of RC girder bridge, known as half-joint bridge.

A half-joint, also known as a ‘Gerber joint’ or dapped-end beam, is a unique type of joint that significantly reduces the depth of a girder or deck at its ends. It is supported by a mirrored cantilevering element. German civil engineer Heinrich Gerber (1832–1912) introduced this

* Corresponding author.
*E-mail address:* paolo.martinelli@polimi.it (P. Martinelli).
[1] https://orcid.org/0000-0003-1029-7744
[2] https://orcid.org/0000-0001-6457-7894
[3] https://orcid.org/0000-0003-1779-2449

https://doi.org/10.1016/j.engstruct.2024.117712
Received 1 December 2023; Received in revised form 8 February 2024; Accepted 18 February 2024

technique, creating an internal hinge in concrete decks or girders, while maintaining a level-running surface. Over the past few decades, half-joint bridges have gained popularity worldwide due to their straightforward design and construction. In Italy, this joint was commonly used from the 1960s to the 1990s. The precise number of half-joint bridges currently in service in Italy is unknown. However, when examining the infrastructure under the management of ASPI (Autostrade Per l'Italia), the primary private company responsible for Italian highways, an internal report from the scientific committee presented in 2022 [22] revealed that out of 1954 bridges with a span length exceeding 10 m, approximately 5% (or about 100 bridges) are constructed with reinforced concrete half-joints. This design solution is no longer adopted in Italy mainly due to water leakage issues causing concrete deterioration and reinforcing steel corrosion. Originally, half-joints were designed exclusively for railway bridges, where water accumulation on the deck was not a significant concern. However, the unique L-shaped geometry of the joint presents challenges for inspections, making it difficult to access the interior and identify deterioration mechanisms and their progression over time. As many half-joint bridges approach the end of their service life, these issues become more prominent, necessitating careful and focused attention.

The Italian Guidelines for the classification, assessment, and management of bridges [23] classify half-joints as 'critical elements'. This term refers to elements that are susceptible to degradation and whose potential failures can significantly affect the overall structural behaviour of the bridge. This work applies a simple methodology based on the notional removal of half-joints for quantifying the structural robustness. A preliminary effort in this regard was undertaken by Martinelli et al. [24]. The Annone viaduct, an RC half-joint bridge that collapsed in 2016 after a heavy truck passed through, resulting in one fatality, is used as a case study. This bridge, constructed in the early 1960s in northern Italy, featured a central suspended span and two side spans with a cantilever scheme, measuring a total length of 56.10 m. An investigation carried out by di Prisco et al. [25] revealed prior damage, deterioration, and design flaws in the half-joints. Furthermore, the bridge faced misuse, such as the passage of heavy trucks, a factor not accounted for in the initial design.

In this paper, Section 2 reviews some established robustness measures from the existing literature. In this work, deterministic indicators for quantifying robustness are intentionally chosen to ensure that they can be readily used by structural engineers without requiring specialized skills in risk analysis. Section 3 provides a description of the case study bridge, highlighting its main geometric features, assumed load configurations, and half-joint resistance. Section 4 describes the linear and nonlinear finite element models. Section 5 presents a notional removal approach applicable to half-joint bridges for quantifying structural robustness. Results are presented and critically discussed in Section 6. Finally, Section 7 draws the main conclusions and practical recommendations.

## 2. Quantification of structural robustness

Objective measures of robustness are required to ensure safety against progressive collapse, estimate potential losses, and make informed decisions regarding the acceptability of a given level of robustness. Additionally, having a quantitative measure of robustness proves invaluable in prioritizing maintenance and repair efforts for existing structures. Various indicators for quantifying robustness are available in the scientific literature. These indicators encompass deterministic, probabilistic, and risk-based formulations. A comprehensive collection of these robustness measures is detailed in [26]. However, it is important to note that a consensus has not yet emerged regarding a single, universally accepted measure of robustness. This lack of unanimity poses challenges to the widespread adoption of robustness indicators.

Deterministic approaches to assess robustness often rely on evaluating the outcomes following an assumed initial structural damage. These measures primarily involve quantifying alterations in critical structural characteristics, such as stiffness or strength. They all share a common principle: comparing the properties of the intact structure with those of the damaged one. While specific robustness indicators tailored for bridges may not exist, an in-depth examination of the metrics found in the literature enables the identification of preferred indicators, depending on the specific collapse mechanisms under consideration [27].

Among the deterministic indicators of robustness that can be computed using linear elastic material behaviour, the 'reserve-based measure' proposed by Starossek [27] and denoted as $R_r$ emerges as particularly well-suited for the examination of half-joint girder bridges. This measure is based on the redistribution of forces that occurs following the failure of a structural element. The term 'reserve-based measure' derives from the fact that force redistribution is only possible when the structure possesses surplus bearing capacity. To illustrate this concept, a scenario where a beam is suspended by rods in its initial intact configuration is considered (Fig. 1a). The applied load induces stresses within the rods. Consider a localized failure occurring in j-th rod. When the j-th rod is eliminated, as illustrated in Fig. 1b, the force previously carried by j-th rod redistributes throughout the system, resulting in an increase $\Delta F_k$ in the force within the adjacent k-th rod. The maximum dynamic force in the k-th rod $F_{kj}$ ($F_{kj} = F_k + \Delta F_{kj}$) can be compared with the bearing capacity of the rod ($F_{k,ult}$). The index $R_r$ can then be expressed as:

$$R_r = 1 - \max_{k,j} \frac{F_k + \Delta F_{kj}}{F_{k,ult}} \tag{1}$$

In this formulation, positive values of $R_r$ signify structural robustness, indicating that failure does not propagate. Conversely, negative values of $R_r$ indicate the potential for progressive collapse and a lack of structural robustness.

Biondini and Restelli [28] have introduced a set of dimensionless robustness indices ($\rho$) within the 0 to 1 range, which are associated with the structural behaviour of linear systems. In this study, we focus on the following specific indices:

$$\rho_T = \frac{T_{n0}}{T_{n1}} \tag{2}$$

In Eq. (2) $T_n$ represents the first natural vibration period of the system, with subscripts '0' and '1' indicating the intact and damaged states of the structure, respectively. Additionally, this study adopts a third indicator associated with the displacements of the systems:

$$\rho_s = \frac{\|s_0\|}{\|s_1\|} \tag{3}$$

where $\rho_s$ is defined as the ratio of the Euclidean scalar norm ($\| \bullet \|$) of the

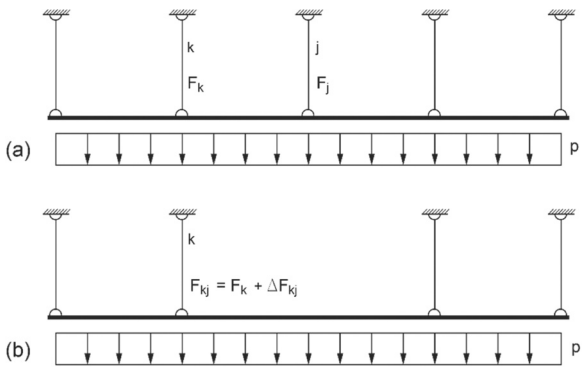


**Fig. 1.** Example of a beam suspended on rods to illustrate the index $R_r$ (adapted from [27]).

displacement vector $\boldsymbol{s}$ in the intact state (subscript '0') to that in the damaged state (subscript '1'). A fourth indicator is considered within this study:

$$\rho_{\Phi} = \frac{\Phi_0}{\Phi_1} \tag{4}$$

Symbol $\Phi$ in Eq. (4) represents the stored energy. This index quantifies the changes in stored energy between the intact state (subscript '0') and the damaged state (subscript '1'). While indices defined in Eqs. (3)–(4) were initially formulated for linear systems, their application can extend to nonlinear systems as well.

The robustness indicators $R_r$, $\rho_s$, and $\rho_{\Phi}$ depend on the specific loading combination considered, making them 'threat-dependent' indicators. In contrast, the indicator $\rho_T$ remains unaffected by the choice of load combination and is therefore referred to as a 'threat-independent' indicator. All four of these aforementioned indices are applied, compared, and discussed within the context of the selected case study, examining notional removal scenarios as described in the following sections.

The index $R_r$ expresses structural redundancy by quantifying the system's capacity to redistribute loads following damage to one or a few structural elements. Additionally, it also represents structural robustness for structures susceptible to zipper-type collapse, such as half-joint RC bridges (readers can refer to [29] for a detailed description of this type of progressive collapse), as susceptibility to zipper-type collapse increases with the system's inability to redistribute loads.

In the literature, terms like structural robustness, redundancy, and static indeterminacy are often used interchangeably, but they represent distinct properties of structural systems. The foundational distinction among these terms is elaborated upon in Biondini et al. [30], which also provides several illustrative examples. It has been demonstrated that the degree of static indeterminacy does not consistently reflect structural redundancy [30,31]. While structural robustness can benefit from redundancy and presence of alternative load paths, an increase in redundancy does not necessarily equate to improved structural robustness [32,33]. In fact, the redistribution of internal forces within a damaged system can contribute to the progression of damage and, consequently, reduce overall robustness.

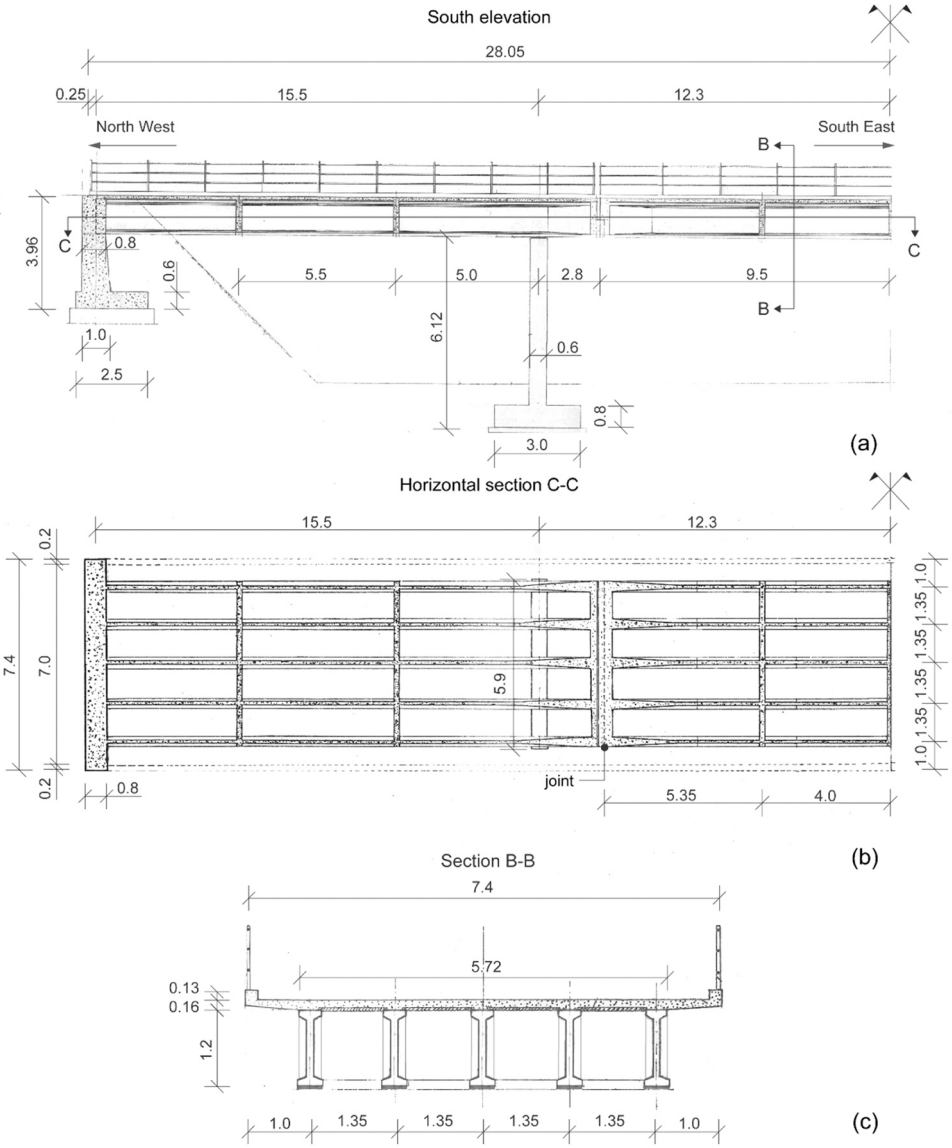


**Fig. 2.** Readjustment of the original design drawings of the bridge: (a) side view, (b) horizontal section and (c) vertical cross-section (units: m; adapted from [25]).

## 3. Case study

### 3.1. Bridge geometry

The bridge case study is the Annone overpass, a precast concrete structure built in the 1960s. Unfortunately, in 2016, it suffered a catastrophic collapse due to shear failure at one of its half-joints while a heavy truck was passing over it. This bridge was located in the village of Annone, within the province of Lecco in northern Italy.

It was originally designed as a second-category bridge under Circular 14 February 1962 No. 384 [34]. The Annone overpass consisted of a central suspended span (referred to as a 'drop-in') flanked by two side spans utilizing a cantilever design. The entire structure had a total length of 56.10 m and a width of 7.4 m, as illustrated in Fig. 2a and Fig. 2b. The two side spans were supported at their ends by abutments and intermediate walls, each featuring a cantilever section of approximately 2.80 m. In the central portion of the bridge, the main beams were supported using half-joints. Each of the two joints of the central suspended span features five Gerber saddles. These central beams had a span of 19.0 m. A horizontal cross-section of the central and side spans is depicted in Fig. 2b. The bridge load-bearing system consisted of five prestressed prefabricated beams (PC beams), spaced at intervals of 1.35 m along the bridge transverse axis. These beams provided support for a continuous cast-in-situ RC slab, as shown in Fig. 2c. The RC top slab was clamped at the abutments. Additionally, RC transversal beams were cast in situ – five in the central span and four in the side spans – running perpendicular to the longitudinal direction of the bridge. For more detailed information about the bridge geometry as well as on the reinforcement details, readers can refer to Refs. [25,35].

### 3.2. Load configurations

This section describes the nominal applied loads acting on the central span elements, encompassing their self-weight and various live load configurations. The total self-weight of the bridge, including safety barriers, pavement, curbs, beams, and the reinforced concrete slab, amounted to 1690 kN, exceeding the designer's assumed value of 1521 kN. The dimensions of standard lanes, load placements, and the naming conventions for the 10 half-joints (R1 – R10) are depicted in Fig. 3, while the load magnitudes and total loads are collected in Table 1 and Table 2.

Five load configurations are considered to maximize the load on supports R1-R5 (symmetrical load configurations with respect to the mid-span can be assumed to maximize the load on supports R6-R10):

1) The first load configuration is illustrated in Fig. 3a, where lane 1 is subjected to the load specifications outlined in Circular 14 February 1962, No. 384 [34]. This results in a total live load of 554.2 kN (see Table 1 and Table 2). This configuration comprises a combination of concentrated loads.
2) The second load configuration, depicted in Fig. 3a, involves loading both lanes 1 and 2 in accordance with Circular 14 February 1962, No. 384 [34]. This leads to a total live load of 1108.4 kN (see Table 1 and Table 2). Similar to the first configuration, it consists of a combination of concentrated loads.
3) The third load configuration, schematically represented in Fig. 3b, includes the application of NTC 2018 [36] specifications (which is the most recent design code in Italy) to lane 1, resulting in a total live load of 1132.0 kN (see Table 1 and Table 2). This configuration combines concentrated and distributed loads.
4) In the fourth load configuration, also illustrated in Fig. 3b, lanes 1 and 2 are both subjected to the load conditions specified in NTC 2018 [36], resulting in a total live load of 1693.5 kN (see Table 1 and Table 2). Like the third configuration, this one involves a combination of concentrated and distributed loads.

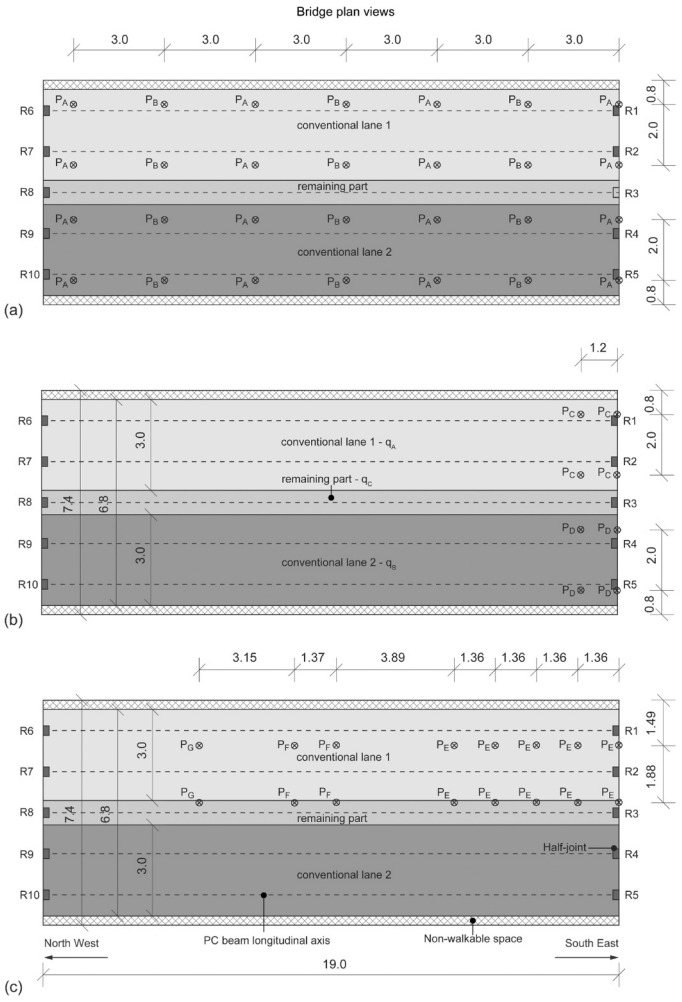


**Fig. 3.** Loads on the bridge central span according to: (a) Circular 14 February 1962 No. 384 [34], (b) NTC 2018 [36] and (c) 8-axle heavy truck.

**Table 1**
Values of loads $P_A$–$P_G$ and $q_A$–$q_C$ indicated in Fig. 3.

| Load | Value |
|---|---|
| $P_A$ (kN) | 50.384 |
| $P_B$ (kN) | 25.192 |
| $P_C$ (kN) | 150.0 |
| $P_D$ (kN) | 100.0 |
| $P_E$ (kN) | 69.651 |
| $P_F$ (kN) | 67.689 |
| $P_G$ (kN) | 44.145 |
| $q_A$ (kN/m$^2$) | 9.0 |
| $q_B$ (kN/m$^2$) | 2.5 |
| $q_C$ (kN/m$^2$) | 2.5 |

**Table 2**
Total live loads in the L1-L5 load configurations.

| Load ID | Load type | Total live load (kN) |
|---|---|---|
| L1 | Fig. 3a – [34] – 1 lane | 554.224 |
| L2 | Fig. 3a – [34] – 2 lanes | 1108.448 |
| L3 | Fig. 3b – [36] – 1 lane | 1132.000 |
| L4 | Fig. 3b – [36] – 2 lanes | 1693.500 |
| L5 | Fig. 3c – heavy truck | 1055.556 |

5) The fifth load configuration, as depicted in Fig. 3c, models the loading of lane 1 by an 8-axle heavy truck, representing the load combination that caused the failure of half-joint R1 and the subsequent bridge collapse. The total live load for this scenario is 1055.6 kN (see Table 1 and Table 2). It is characterized by a combination of concentrated loads.

The bridge was designed according to the guidelines specified in Circular 14 February 1962, No. 384 [34], categorizing it as a second-category bridge. As a result, load combinations 1 and 2 represent the designated load combinations for the design. For load combinations 1 and 2, it was assumed that the distance between two consecutive vehicles was zero. The amplitudes provided in Table 1 for load combinations 1 and 2 account for the effect of a dynamic amplification factor (DAF) expressed as follows in [34]:

$$\mathrm{DAF} = 1 + \frac{(100 - L)^2}{100(250 - L)} = 1.284 \tag{5}$$

where in Eq. (5) $L$ represents the distance between supports in meters ($L$ = 19 m for the central span). It should be emphasized that the live loads associated with load combinations 3–5 are significantly higher than those envisaged in the design phase.

### 3.3. Half-joint resistance

Eq. (1) necessitates determining the ultimate capacity ($F_{k,ult}$) of half-joints, which serve as critical components in the overall system. The estimation of $F_{k,ult}$ relies on strut-and-tie models, as described in di Prisco et al. [25] and here omitted for the sake of brevity. These models accurately reproduce the geometric characteristics and reinforcement details of the half-joints. Concerning reinforcement details, the analysis assumes nominal bar diameters in the as-built condition. Consequently, the calculated ultimate load capacity for each half-joint is 578.5 kN, assuming the experimental average value of the ultimate strength for the definition of reinforcement tie contribution.

## 4. Finite element models

Robustness quantification is conducted through the utilization of both linear elastic (see Section 4.1) and simplified nonlinear (see Section 4.2) finite element (FE) models. The geometric parameters of these FE models are derived from the original design report and associated structural drawings. Subsequently, the FE models are constructed and analysed within the ABAQUS/Standard environment [37].

### 4.1. Linear elastic model

The reference intact model employed in this study, denoted as 'num. 2 A', is nearly identical to the one described in di Prisco et al. [25], with the only difference being a denser mesh featuring an average mesh side of 100 mm.

Key characteristics of this model are summarized here; for a detailed description, readers are directed to [25]. It is a simplified 3D model that excludes the side spans, focusing exclusively on the central span of the bridge. Fig. 4a and Fig. 4b offer an overall view of the bridge, highlighting the central span with a grey background and a dashed rectangle. The side spans are treated as elastic constraints for the central span, as illustrated in the loading scheme shown in Fig. 4c. In this scheme, a stiffness of $k$ = 6.06E7 N/m is determined for the PC beams and the top slab, utilizing the elastic constants reported in [25]. However, this value of $k$ does not account for the redistribution and stiffening effect of the transversal beams. Validation of the simplified model in terms of forces transmitted to Gerber saddles against values obtained with a full model was carried out in a previous study [25] and is not repeated here.

Elastic constraints, specifically translational springs in the Y direction, are applied to the ends of the central span beams, as depicted in Fig. 4d. Fig. 4e provides a 3D mesh view of the simplified FE model. Two distinct types of 3D finite elements are used to discretize different regions of the bridge. Shell-type elements (finite element S4R) with four nodes and 6 degrees of freedom per node are employed for the top RC slab. Linear beam-type elements (finite element B31) with two nodes and 6 degrees of freedom per node are applied to the longitudinal and transversal beams. The geometric attributes of the longitudinal and transversal beams, including area, second moment of area, and torsional inertia, are derived from the design report, with an assumption of uniform cross-sections in the end sections of the longitudinal beams. The model assumes full continuity between longitudinal and transversal beams. Overall, the FE model comprises 16234 nodes and 15979 elements, consisting of 1195 beam-like elements and 14784 shell-like elements.

The connection between the lower lattice, composed of longitudinal PC beams and transversal RC beams, and the upper slab is implemented

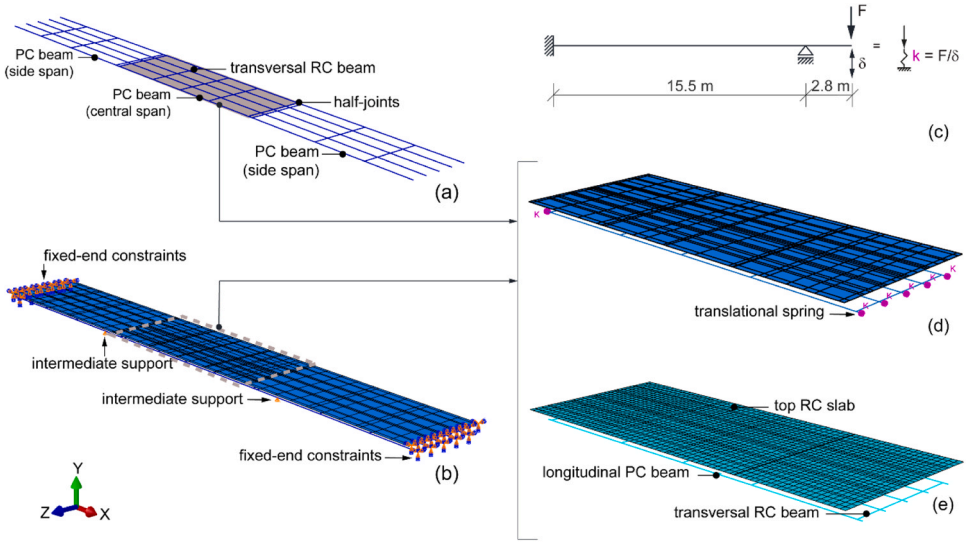


**Fig. 4.** Complete FE model: (a) particular of the longitudinal and transversal beams and (b) details of the boundary conditions. Simplified FE model: (c) lateral span loading scheme used for estimating the stiffness (k) of half-joints (d) details of the boundary conditions and (e) mesh view (adapted from [25]).

by using kinematic couplings that restrict movement in all six degrees of freedom, constraining the upper portion of the beams to the lower part of the slab. This interaction mechanism enables the transfer of torsional forces from the slab to the beams, aligning with the construction method employed for the overpass.

The materials are assumed to be in a linear elastic state without cracks, and the FE models do not include steel reinforcement. Details on the elastic constants for PC beams, transversal RC beams, and the top RC slab can be found in di Prisco et al. [25].

### 4.2. Simplified nonlinear model

The structural misconception of Gerber saddles causes these elements to function as structural fuses. The comparison of internal forces/moments in both PC beams and RC slab, under loading conditions L1-L5 (as described in Fig. 3) and the resisting capacity of the respective cross-sections, reveals an almost elastic material behaviour. This is except for the half-joint regions. This outcome validates the development of simplified nonlinear models, concentrating the nonlinear behaviour exclusively in the half-joint regions. Under all loading conditions, the moments acting in the longitudinal and transverse beams never exceed their resisting counterparts. Specifically, the moment acting on the main beams ensures the beams remain within the elastic phase of the sectional response. Additionally, the shear force in both longitudinal and transverse beams consistently remains below their resisting capacity. Although in very limited regions close to the concentrated loads or near the half-joints, the acting transverse moment per unit length applied on the top RC slab exceeds the resisting ones, these effects are considered negligible.

Nonlinearity is addressed through the incorporation of a macroscopic phenomenological model, which involves replacing the linear spring used in model 'num. 2 A' (Section 4.1; Fig. 4d) with a nonlinear translation spring. The development of refined three-dimensional nonlinear FE models for critical sections of the bridge is beyond the scope of this study.

The description of the nonlinear spring behaviour follows the approach outlined in [25], with essential points reiterated below. The translational spring is of the compression-only multilinear type, and its nonlinear load-displacement ($P$-$\delta$) behaviour is derived from the cracking pattern and rigid body motion, as shown in Fig. 5a. The relationship between vertical deflection ($\delta_w$) and crack opening ($w$) is illustrated in the same figure. The overall displacement response ($\delta$) comprises two components: the elastic deflection of the side PC beam ($\delta_b$ in Fig. 5b) and the rigid body motion, resulting from the cracking occurring in the half-joint ($\delta_w$ in Fig. 5b). All rebars in the half-joint are assumed to be non-corroded (labelled as 'NC' in [25]). The definition of the nonlinear $P$-$\delta$ relationship involves calculating the yielding load ($P_y$), ultimate load ($P_u$), and ultimate displacement ($\delta_u$), as depicted in Fig. 5b. The numerical model maintains the same initial stiffness ($k$) as provided in Section 4.1 (i.e., branch OA in Fig. 5b). The loads corresponding to $P_y$ and $P_u$ are determined from the strut-and-tie cases C and D as identified in [25]. The ultimate crack opening ($w_u$), used to define $\delta_u$, is computed following the guidelines outlined in *fib* Model Code 2010 [38] and *fib* Bulletin 63 [39]. For a comprehensive derivation of $w_u$, readers are directed to Ref. [25]. The BC branch is introduced to nullify the contribution of the spring once the ultimate load $P_u$ is reached. Detailed values describing the force-displacement behaviour of Gerber saddles are listed in Table 3. The assumption of uncorroded bars implies elasto-plastic behaviour in half-joints (Fig. 5b). Conversely, the presence of corrosion could embrittle the behaviour of the half-joints. In such instances, the initiation of transverse redistribution of loads due to half-joint loss may contribute to damage progression, consequently reducing the overall robustness.

## 5. Notional removal approach for half-joint girder bridges

The design resulting from actions caused by unspecified hazards can be addressed using a notional damage scenario approach. According to the draft version of the *fib* Model Code 2020 document [40], notional damage scenarios can encompass either (i) notional deterioration scenarios or (ii) notional removal scenarios. In case (i), the geometrical and/or material properties of one or more structural elements are notionally reduced, and the structure is then checked for disproportionate consequences. In case (ii), structural elements are notionally removed, and the structure is evaluated for disproportionate consequences. This evaluation may include the conducting an alternative load path design. Structural elements, such as one or more columns, panels/walls, or nominal wall lengths, along with any other elements deemed vital to structural performance, can be notionally removed.

Notional removal scenarios, typically associated with connection or structural member failures resulting from unidentified hazards, have been widely employed to assess the robustness of buildings (see, for example, Refs. [41–43], among others). The notional removal scenarios strategy is being applied to the bridge under study by removing the half-joints, specifically the lower nib of the half-joint of the side span PC beams. The scenarios to be considered involve the removal of one half-joint at a time, as illustrated in Fig. 6 for the removal of half-joint R3 taken as an example. It is worth noting that the notional removal scenario approach adopted here is more conservative than the notional

**Table 3**
Simplified nonlinear behaviour for half-joints R1-R10 in terms of load vs displacement (points O, A, B and C indicated in Fig. 5b).

| Point | Displacement δ | Load P |
|---|---|---|
| | (m) | (N) |
| O | 0 | 0 |
| A | $5.886 \times 10^{-3}$ | 356700 |
| B | $55.676 \times 10^{-3}$ | 578500 |
| C | $57.0 \times 10^{-3}$ | 0 |

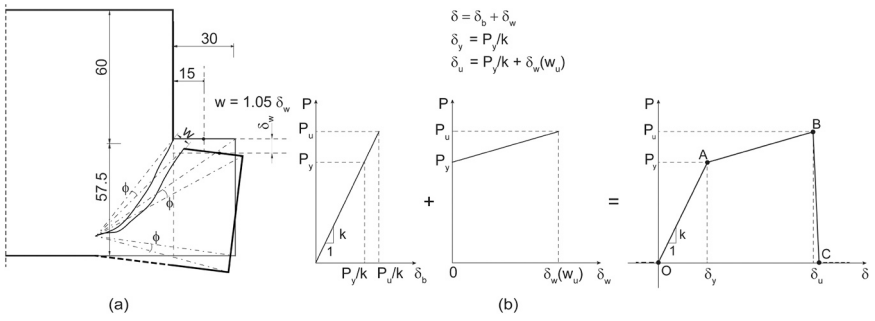


**Fig. 5.** (a) schematic cracking pattern and rigid body motion of half-joint R1 at the onset of collapse and (b) simplified nonlinear behaviour for half-joints R1-R10 (length in centimetres;
adapted from [25]).

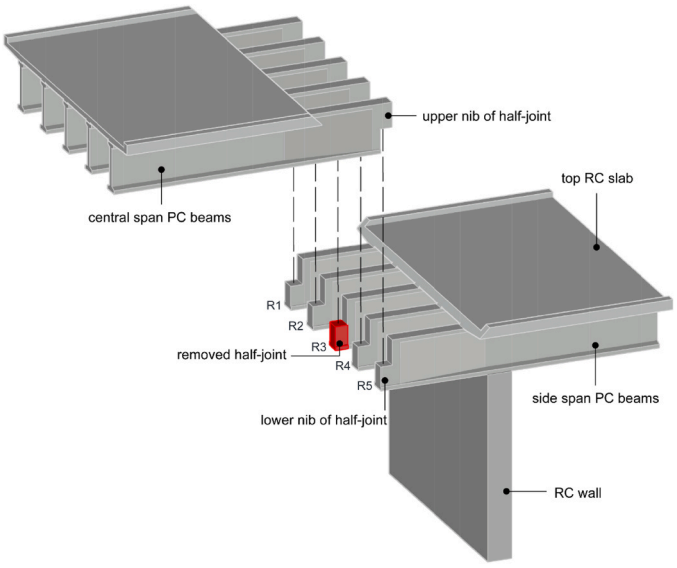


**Fig. 6.** Schematic representation of one generic half-joint loss scenario.

deterioration scenario approach, because the whole structural element is removed and not only a reduction of stiffness and/or bearing capacity is considered.

Due to the symmetry of the loads outlined in Section 3.2 concerning the centreline of the bridge, it is adequate to consider the loss of half-joints R1-R5 (e.g., loss of half-joint R1, loss of half-joint R2, and so forth). As illustrated in Fig. 6, an example of this is the loss of half-joint R3, highlighted in red.

The collapse of half-joints in bridges can be caused by various reasons. Some of the common factors that can lead to the collapse of half-joints, not in order of importance, include:

1) Overloading: the application of excessive load on the structure can cause the collapse of half-joints. This overloading can be caused by factors such as heavy traffic, wind, accumulated snow, or concentrated loads.
2) Lack of maintenance: the absence of regular maintenance can lead to the deterioration of structural components, including half-joints. Corrosion, rust, or other damage can weaken the structure over time, increasing the risk of collapse.
3) Design or construction defects: errors in design or construction execution can negatively impact the stability of half-joints and the overall structure.
4) Low-quality materials: the use of low-quality materials or materials that do not meet safety standards can contribute to the failure of half-joints and the vulnerability of the structure.
5) Operational errors: human errors in the management and use of the bridge, such as deliberate overloading or improper use, can lead to the failure of half-joints.

Factors 1, 2, 3, and 5 contributed to the collapse of the Annone viaduct. It is evident that some of these causes could also inflict partial damage on other parts of the bridge. Therefore, assuming the loss of half-joints, while keeping the remaining bridge sections intact is a common and convenient simplification during the design phases.

Table 4 summarizes the key attributes of both static linear and nonlinear analyses. The model ID indicates the removed half-joint position (R1 to R5, including the intact situation labelled as 'INTACT') and the load configurations (L1 to L5). Additionally, it indicates the presence or absence of mechanical nonlinearity, distinguishing between the linear elastic model ('L') and the nonlinear model ('NL').

## 6. Results and discussion

The FE models described in Section 4 enable the calculation of the $R_r$, $\rho_T$, $\rho_S$ and $\rho_\Phi$ indices, as defined in Eqs. (1) to (4). When considering linear elastic analyses, Fig. 7a-e examine the load configurations L1-L5, as outlined in Section 3.2. These figures depict the reactions in half-joints R1-R5 for both the intact situation and various half-joint loss scenarios explained in Section 5. In Fig. 7, a horizontal dashed line is used to define the ultimate capacity of the half-joint (see Section 3.3). As one would logically expect, the reaction in a removed half-joint is zero. Load configuration L2, which exhibits symmetry in the transverse direction of the bridge (as seen in Fig. 3a), results in a force distribution in the half-joints that is symmetric in the transverse direction (Fig. 7b). Load configurations L1 and L2, representing the loads prescribed during the design phase, show that the loads transmitted to the half-joints do not exceed the ultimate capacity even in the event of a single half-joint loss (Fig. 7a-b). In contrast, load configurations L3-L5, representing abnormal/heavier loading conditions than those predicted in the design phase, lead to the exceedance of the half-joint's ultimate capacity for various half-joint loss scenarios (Fig. 7c-e).

Fig. 7 illustrates that the most severe condition occurs when the end half-joint R1 in lane 1 is removed. In this scenario, the adjacent half-joint R2 registers the maximum reaction. Another significant load condition, in comparison to the intact condition, is the loss of half-joint R2 for all the examined load configurations. When loads are applied to both lanes (Fig. 7b and Fig. 7d), a similarly critical load condition, compared to the intact condition, is the loss of the other end half-joint R5. The removal of the centre half-joint R3 – and to a lesser extent, the inner half-joints R2 and R4 – allows for a more homogeneous redistribution of reactions, making these scenarios less critical than the loss of the end half-joints.

Turning to the analysis of the results from nonlinear models, Fig. 8 depicts the reactions in half-joints R1-R5 for various half-joint loss scenarios, including the intact situation. Subplots (a) to (e) correspond to load configurations L1-L5, respectively. Fig. 8 confirms the findings obtained from the linear models. Specifically, the ultimate capacity of the half-joint is never reached in the L1 and L2 load configurations, regardless of the half-joint loss scenarios (Fig. 8a-b). In the load configuration L3, the loss of half-joint R1 results in the ultimate load reaching the neighbouring half-joint R2, and conversely, the loss of half-joint R2 results in the ultimate load reaching the neighbouring half-joint R1 (Fig. 8c). In the load configuration L4, in four out of five scenarios (except for half-joint loss R4), the loss of a half-joint leads to the ultimate load reaching the neighbouring half-joint. Finally, in the load configuration L5, the loss of half-joint R1 results in the ultimate load reaching the neighbouring half-joint R2.

In all scenarios where the loss of a half-joint leads to reaching the ultimate carrying capacity in the adjacent half-joint, the analysis stops due to a lack of convergence (indicated with a blank circle in Fig. 8). The absence of system equilibrium may be associated with bridge collapse. These scenarios are summarized in Table 5, along with the load multiplier (α) associated with the ultimate load step, which is always less than one. The nonlinear analyses reveal that a bridge, upon losing one half-joint, may redistribute load to prevent collapse in specific scenarios. However, in other cases (as indicated in Table 5), achieving load-bearing capacity in a second half-joint always results in an overall loss of equilibrium, leading to structure collapse.

In framed buildings, the mechanisms that provide alternative load paths and minimize the risk of progressive collapse in case of column loss typically include (a) the catenary/membrane behaviour of beams/slabs, (b) the arch effect of the beams, (c) the Vierendeel behaviour of the frame, and (d) the contribution of non-structural elements [26]. However, in the case of the half-joint RC girder bridge under study, the resisting mechanism that emerges after the loss of a half-joint involves the flexural-transverse and torsional stiffness provided by the beam grid and top slab. This stiffness facilitates the redistribution of the load to adjacent Gerber saddles.

**Table 4**
Main features of finite element models.

| Model ID [half-joint loss - load configuration - mech. nonl.] | Half-joint loss | Load configuration | Mechanical nonlinearity |
|---|---|---|---|
| INTACT-L1-L | none | Fig. 3a – [34] – 1 lane | NO |
| R1-L1-L | R1 | Fig. 3a – [34] – 1 lane | NO |
| R2-L1-L | R2 | Fig. 3a – [34] – 1 lane | NO |
| R3-L1-L | R3 | Fig. 3a – [34] – 1 lane | NO |
| R4-L1-L | R4 | Fig. 3a – [34] – 1 lane | NO |
| R5-L1-L | R5 | Fig. 3a – [34] – 1 lane | NO |
| INTACT-L2-L | none | Fig. 3a – [34] – 2 lanes | NO |
| R1-L2-L | R1 | Fig. 3a – [34] – 2 lanes | NO |
| R2-L2-L | R2 | Fig. 3a – [34] – 2 lanes | NO |
| R3-L2-L | R3 | Fig. 3a – [34] – 2 lanes | NO |
| R4-L2-L | R4 | Fig. 3a – [34] – 2 lanes | NO |
| R5-L2-L | R5 | Fig. 3a – [34] – 2 lanes | NO |
| INTACT-L3-L | none | Fig. 3b – [36] – 1 lane | NO |
| R1-L3-L | R1 | Fig. 3b – [36] – 1 lane | NO |
| R2-L3-L | R2 | Fig. 3b – [36] – 1 lane | NO |
| R3-L3-L | R3 | Fig. 3b – [36] – 1 lane | NO |
| R4-L3-L | R4 | Fig. 3b – [36] – 1 lane | NO |
| R5-L3-L | R5 | Fig. 3b – [36] – 1 lane | NO |
| INTACT-L4-L | none | Fig. 3b – [36] – 2 lanes | NO |
| R1-L4-L | R1 | Fig. 3b – [36] – 2 lanes | NO |
| R2-L4-L | R2 | Fig. 3b – [36] – 2 lanes | NO |
| R3-L4-L | R3 | Fig. 3b – [36] – 2 lanes | NO |
| R4-L4-L | R4 | Fig. 3b – [36] – 2 lanes | NO |
| R5-L4-L | R5 | Fig. 3b – [36] – 2 lanes | NO |
| INTACT-L5-L | none | Fig. 3c – Heavy truck | NO |
| R1-L5-L | R1 | Fig. 3c – Heavy truck | NO |
| R2-L5-L | R2 | Fig. 3c – Heavy truck | NO |
| R3-L5-L | R3 | Fig. 3c – Heavy truck | NO |
| R4-L5-L | R4 | Fig. 3c – Heavy truck | NO |
| R5-L5-L | R5 | Fig. 3c – Heavy truck | NO |
| INTACT-L1-NL | none | Fig. 3a – [34] – 1 lane | YES |
| R1-L1-NL | R1 | Fig. 3a – [34] – 1 lane | YES |
| R2-L1-NL | R2 | Fig. 3a – [34] – 1 lane | YES |
| R3-L1-NL | R3 | Fig. 3a – [34] – 1 lane | YES |
| R4-L1-NL | R4 | Fig. 3a – [34] – 1 lane | YES |
| R5-L1-NL | R5 | Fig. 3a – [34] – 1 lane | YES |
| INTACT-L2-NL | none | Fig. 3a – [34] – 2 lanes | YES |
| R1-L2-NL | R1 | Fig. 3a – [34] – 2 lanes | YES |
| R2-L2-NL | R2 | Fig. 3a – [34] – 2 lanes | YES |
| R3-L2-NL | R3 | Fig. 3a – [34] – 2 lanes | YES |
| R4-L2-NL | R4 | Fig. 3a – [34] – 2 lanes | YES |
| R5-L2-NL | R5 | Fig. 3a – [34] – 2 lanes | YES |
| INTACT-L3-NL | none | Fig. 3b – [36] – 1 lane | YES |
| R1-L3-NL | R1 | Fig. 3b – [36] – 1 lane | YES |
| R2-L3-NL | R2 | Fig. 3b – [36] – 1 lane | YES |
| R3-L3-NL | R3 | Fig. 3b – [36] – 1 lane | YES |
| R4-L3-NL | R4 | Fig. 3b – [36] – 1 lane | YES |
| R5-L3-NL | R5 | Fig. 3b – [36] – 1 lane | YES |
| INTACT-L4-NL | none | Fig. 3b – [36] – 2 lanes | YES |
| R1-L4-NL | R1 | Fig. 3b – [36] – 2 lanes | YES |
| R2-L4-NL | R2 | Fig. 3b – [36] – 2 lanes | YES |
| R3-L4-NL | R3 | Fig. 3b – [36] – 2 lanes | YES |
| R4-L4-NL | R4 | Fig. 3b – [36] – 2 lanes | YES |
| R5-L4-NL | R5 | Fig. 3b – [36] – 2 lanes | YES |
| INTACT-L5-NL | none | Fig. 3c – Heavy truck | YES |
| R1-L5-NL | R1 | Fig. 3c – Heavy truck | YES |
| R2-L5-NL | R2 | Fig. 3c – Heavy truck | YES |
| R3-L5-NL | R3 | Fig. 3c – Heavy truck | YES |
| R4-L5-NL | R4 | Fig. 3c – Heavy truck | YES |
| R5-L5-NL | R5 | Fig. 3c – Heavy truck | YES |

Fig. 9 displays the robustness index $R_r$ calculated using Eq. (1). Negative values of $R_r$ indicate that at least one of the structural elements exceeds its bearing capacity and therefore a lack of structural robustness for various half-joint loss scenarios and load configurations. For load configurations L1 and L2, positive $R_r$ values are obtained for all half-joint loss scenarios. In the case of load configuration L3, positive $R_r$ values are obtained for half-joint losses R4 and R5. In load configuration L4, positive $R_r$ values are obtained only when half-joint R4 is removed. Lastly, in load configuration L5, positive $R_r$ values are obtained for half-joint losses R3 to R5. In all load configurations, consistent with the results in Fig. 7 and Fig. 8, the most critical scenario is the loss of half-joint R1. It is important to note that for load configurations L1 and L2 (loads defined as per Circular 14 February 1962 No. 384 [34], and for which the bridge was designed), the loss of a single half-joint does not lead to a failure propagation.

Fig. 10 presents the robustness index $\rho_T$ calculated using Eq. (2) for various half-joint loss scenarios. The index, which depends only on the natural frequency of the system and is independent of the loading configuration, remains close to unity for all the analysed half-joint removal scenarios. This outcome can be attributed to the minimal

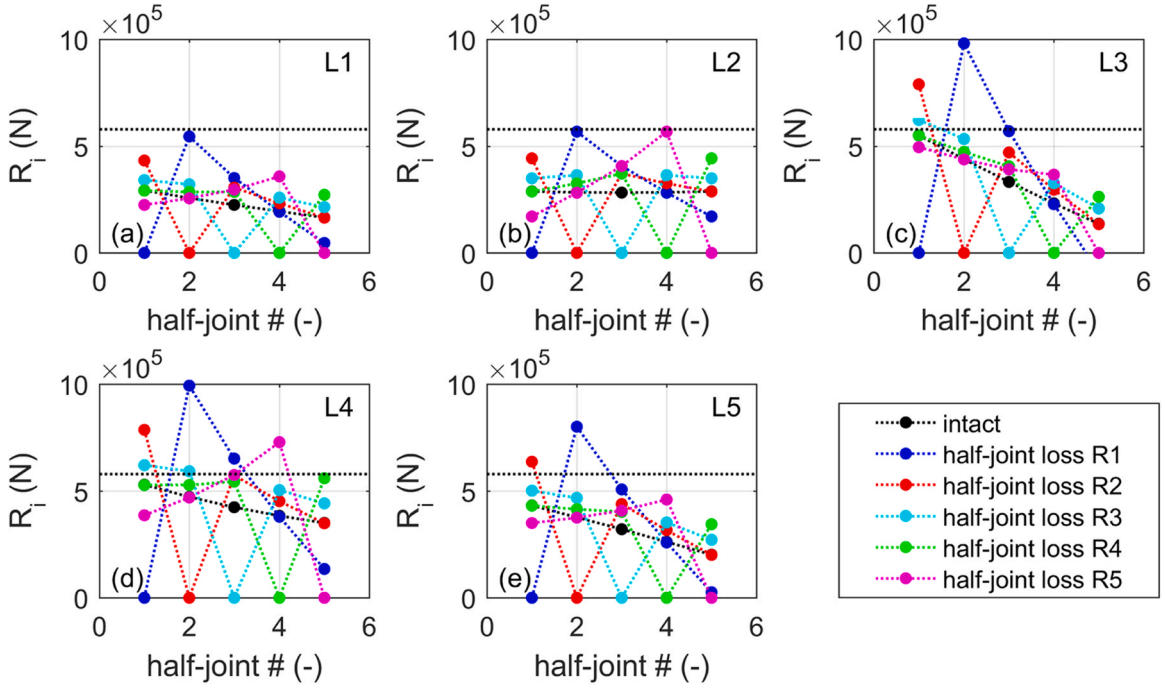


**Fig. 7.** Reactions in half-joints R1-R5 for various half-joint loss scenarios, including the intact situation: (a-e) load configurations L1-L5 (linear elastic models).

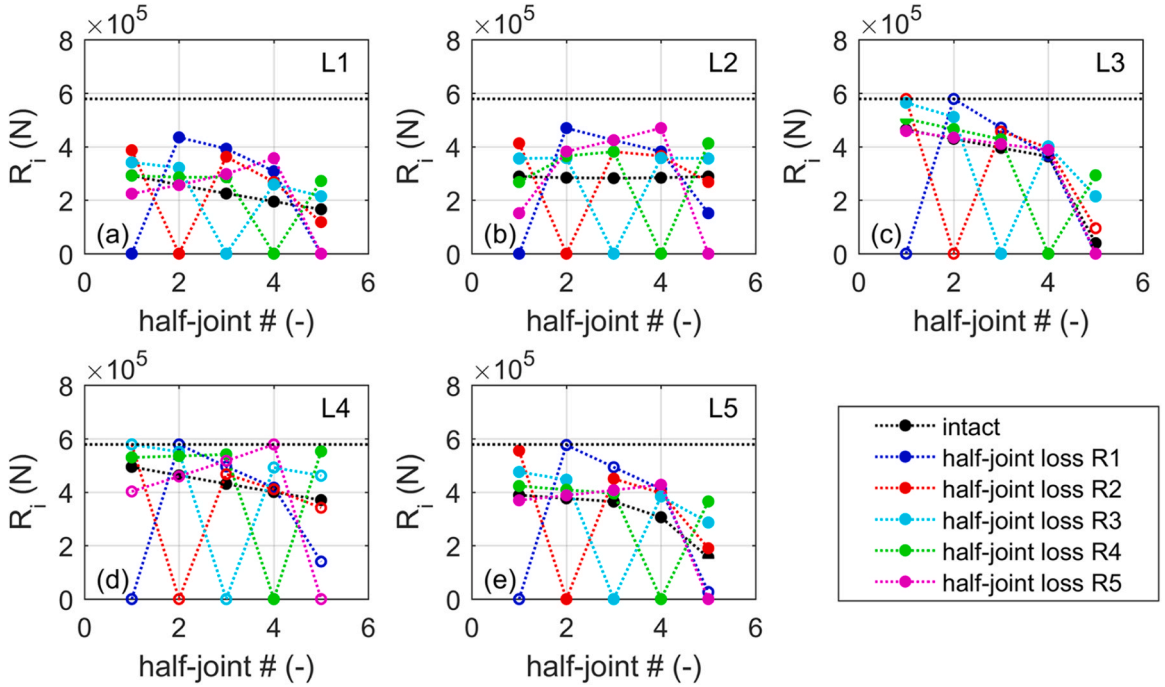


**Fig. 8.** Reactions in half-joints R1-R5 for various half-joint loss scenarios, including the intact situation: (a-e) load configurations L1-L5 (nonlinear models).

variation in stiffness between the intact and damaged system, primarily because of the high stiffness of the deck integrated with the longitudinal and transverse beams, as well as the elastic approach used to describe the deck.

Fig. 11 illustrates the robustness index $\rho_s$ for various half-joint loss scenarios and load configurations. The index $\rho_s$ is calculated using Eq. (3) based on the midspan vertical displacement of the central PC beam, which is considered representative of the overall bridge behaviour. The figure depicts an index close to unity, indicating high robustness, regardless of the removed half-joint or the assumed loading configuration. This result, obtained through linear elastic analyses, can be attributed to the limited impact of losing one out of the ten supports (five supports for each of the two joints) in a highly rigid deck on the midspan central displacement of the central PC beam. Fig. 12 presents the robustness index $\rho_\Phi$ calculated using Eq. (4) for various half-joint loss scenarios and load configurations. The results in Fig. 12 resemble those

**Table 5**
Value of load multiplier for nonlinear analyses that do not reach convergence.

| Model ID [half-joint loss - load configuration - mech. nonl.] | load multiplier α (-) |
|---|---|
| R1-L3-NL | 0.676 |
| R2-L3-NL | 0.806 |
| R1-L4-NL | 0.599 |
| R2-L4-NL | 0.725 |
| R3-L4-NL | 0.942 |
| R5-L4-NL | 0.847 |
| R1-L5-NL | 0.890 |

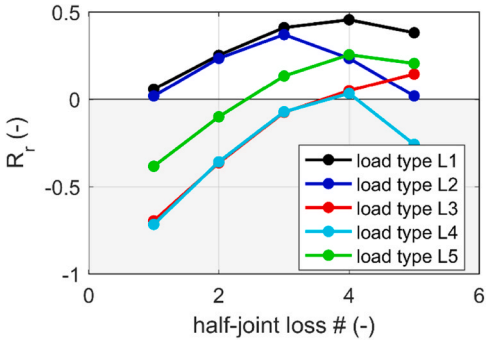


**Fig. 9.** Robustness index $R_r$ for various half-joint loss scenarios and load configurations L1-L5 (linear elastic models).

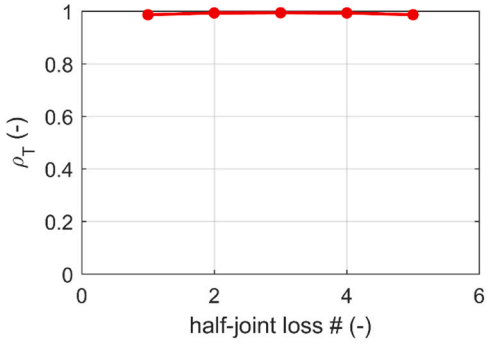


**Fig. 10.** Robustness index $\rho_T$ for various half-joint loss scenarios (linear elastic models).

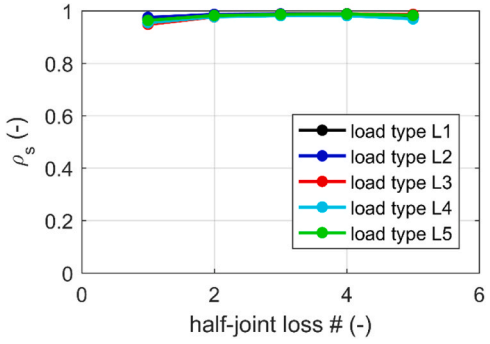


**Fig. 11.** Robustness index $\rho_s$ for various half-joint loss scenarios and load configurations L1-L5 (linear elastic models).

previously shown in Fig. 11, although it is quite evident that the loss of half-joint R1 represents the most unfavourable condition, with $\rho_\Phi$ values ranging from 0.85 to 0.96.

The limited sensitivity of $\rho_s$ and $\rho_\Phi$ to various half-joint removal

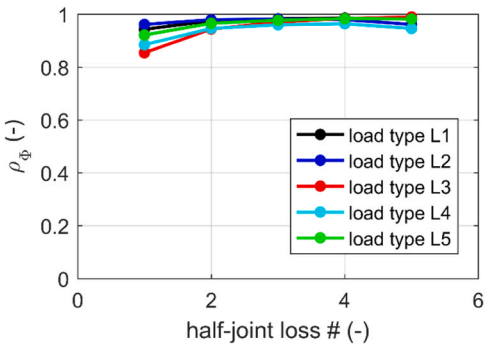


**Fig. 12.** Robustness index $\rho_\Phi$ for various half-joint loss scenarios and load configurations L1-L5 (linear elastic models).

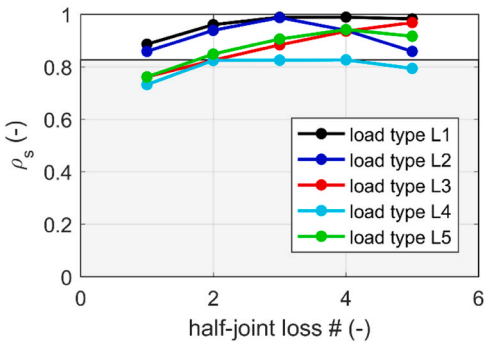


**Fig. 13.** Robustness index $\rho_s$ for various half-joint loss scenarios and load configurations L1-L5 (nonlinear models).

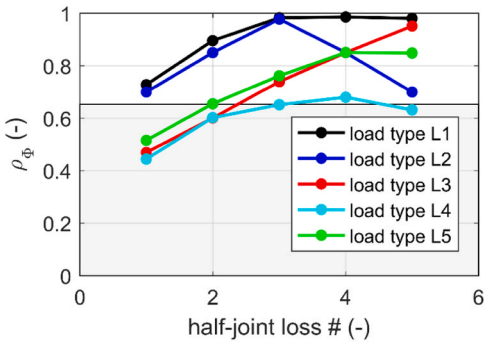


**Fig. 14.** Robustness index $\rho_\Phi$ for various half-joint loss scenarios and load configurations L1-L5 (nonlinear models).

scenarios and loading configurations, suggests recalculating these indicators using nonlinear analyses as presented in Section 4.2. The robustness indices $\rho_s$ and $\rho_\Phi$ for different half-joint loss scenarios and load configurations are displayed in Fig. 13 and Fig. 14, respectively. Nonlinearity in half-joints influences the overall bridge behaviour in both intact and damaged conditions, affecting control point displacement and energy dissipation. This leads to greater variability in $\rho_s$ and $\rho_\Phi$ compared to cases where linear elastic analyses are employed. In Fig. 13 and Fig. 14, the shaded area identifies scenarios where a half-joint has reached its bearing capacity, resulting in analysis convergence failure. In such scenarios, the entire structure is likely to collapse, demonstrating that localized damage accumulated in a half-joint can lead to a disproportionate bridge collapse. The results in Fig. 13 and Fig. 14 exhibit similar trends, with the main difference being that the $\rho_s$ indicator is flattened more than the $\rho_\Phi$ indicator. For the indicator $\rho_s$ (Fig. 13), the threshold that distinguishes potential progressive collapse from

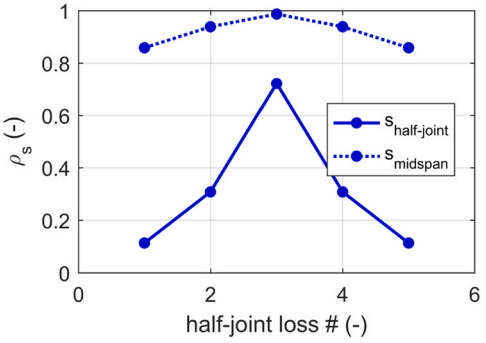


**Fig. 15.** Influence of the displacement chosen for assessing the robustness index $\rho_s$ across different half-joint loss scenarios and load configuration L2 in nonlinear models.

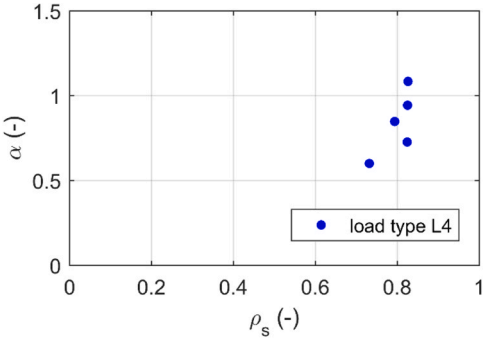


**Fig. 16.** Robustness index $\rho_s$ vs load multipliers $\alpha$ for various half-joint loss scenarios and load configuration L4 (nonlinear models).

situations where it does not occur is relatively high at 0.83, while for the indicator $\rho_\Phi$ (Fig. 14), this threshold is around 0.65. The general findings shown in Fig. 13 and Fig. 14 align with those presented in Fig. 9, which used a different indicator and linear elastic analyses.

Fig. 15 illustrates the impact of the chosen displacement on the assessment of the robustness index $\rho_s$ across various half-joint loss scenarios and load configuration L2 in nonlinear models. The index $\rho_s$ is recalculated using the vertical displacement of the removed half-joint (labelled as '$s_{half-joint}$' in Fig. 15) following Eq. (3). As one would intuitively expect, selecting the displacement across the removed saddle significantly reduces the $\rho_s$ value compared to the situation in which the midspan displacement is chosen (labelled as '$s_{midspan}$' in Fig. 15). The comparison in Fig. 15 highlights the high sensitivity of the indicator $\rho_s$ to the choice of displacement used in Eq. (3).

Fig. 16 illustrates the relationship between the robustness index $\rho_s$ and the collapse multiplier $\alpha$ for different half-joint loss scenarios,

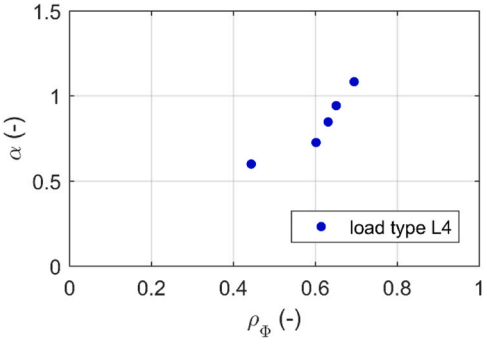


**Fig. 17.** Robustness index $\rho_\Phi$ vs load multipliers $\alpha$ for various half-joint loss scenarios and load configuration L4 (nonlinear models).

considering the heaviest load configuration (L4). Interestingly, it is observed that different half-joint loss scenarios, each associated with a distinct load multiplier, correspond to a very similar robustness index value (around 0.8). Similarly, Fig. 17 displays the robustness index $\rho_\Phi$ vs. load multipliers $\alpha$ for various half-joint loss scenarios and load configuration L4. In this case, there is a direct proportionality between the load multiplier and the robustness index. As $\rho_\Phi$ increases, the value of the load multiplier at collapse also increases.

## 7. Conclusions

In this paper, four deterministic measures of robustness, typically adopted for buildings, are applied to a specific type of reinforced concrete (RC) girder bridge, specifically half-joint bridges. A simple methodology based on the notional removal of half-joints, representing the critical elements for this type of bridge, is applied. The analysis of the structural system under notional removal scenarios is executed through linear and nonlinear static analyses where dynamic effects are neglected. The Annone viaduct, an RC half-joint bridge that collapsed in 2016 after the passage of a heavy truck, is used as a case study. Five load configurations are considered in quantifying the structural robustness: two of them are representative of design loads and the other three are representative of abnormal loads. Based on the results presented, the following conclusions can be drawn.

Given the distinct characteristics of the structure – a bridge featuring a rigid deck integrated with longitudinal and transverse beams – certain robustness indices, specifically the $R_r$, $\rho_s$, and $\rho_\Phi$ indicators, prove more suitable than others. While linear elastic analyses assess the former, the latter two, examined through nonlinear analyses (with mechanical nonlinearity solely included in half-joints), identify similar potential situations of progressive collapse. On the other hand, the indicator $\rho_T$, which is independent of the load configuration, and the indicators $\rho_s$ and $\rho_\Phi$ assessed via linear analysis, are not recommended, as they tend to yield values close to unity for all the half-joint loss scenarios considered. This is primarily because the substantial transverse stiffness of the bridge deck slightly affects the overall elastic response when one support is lost. This observation is also reflected in the results of the index $\rho_T$, which is based on the natural frequency of the structure.

The study emphasizes the importance of establishing a threshold within the range of robustness indices, which typically fall between 0 and 1 (i.e. $\rho_T$, $\rho_s$, and $\rho_\Phi$), to differentiate between robust conditions and potential situations of progressive collapse. This determination can only be made through a careful examination of the structural analysis results.

In the case of the $\rho_s$ index, it is important to point out that designers should pay attention in considering low values of this index as a clear indication of lack of robustness. In fact, a structure experiencing significant displacement due to an accidental event might trigger alternative resistance mechanisms, allowing it to reach equilibrium with the applied load and avoid global failure. Conversely, a brittle collapse mechanism can occur even with minor displacement, resulting in a high $\rho_s$ value. The results have also demonstrated that this index is highly sensitive to the choice of the displacement used in its definition. Global parameters may not accurately reflect the severity of the damage; conversely, selecting a local displacement requires a priori knowledge of the most critical element.

In the case of the half-joint RC girder bridge under study, the established resistance mechanism following the loss of a half-joint relies on the flexural-transverse and torsional stiffness of the beam grid and top slab, facilitating load redistribution to adjacent half-joints. This is further influenced by the presence of five Gerber saddles in the transverse direction at each joint of the central suspended span. While the loss of a Gerber saddle does not invariably lead to the overall collapse of the structure, the attainment of ultimate capacity in a second Gerber saddle always results in the collapse of the entire central span. It is evident that the capacity to redistribute loads in the transverse direction to

neighbouring Gerber saddles is limited or compromised in bridges with just one or two Gerber saddles in the transverse direction.

The results demonstrate a higher level of robustness when internal half-joints are removed, as opposed to the removal of end half-joints. In the former case, the loss of an internal half-joint is generally followed by a redistribution of forces in adjacent Gerber saddles that do not propagate the initial damage across most of the load configurations. On the other hand, the loss of an end half-joint results in a lack of robustness for all considered abnormal load configurations. This finding aligns with the requirements imposed on certain bridges, where the transit of exceptionally heavy trucks must occur in the centre of the roadway. This requirement was also in place for the Annone bridge, but it was unfortunately disregarded by the heavy truck that led to the rupture of half-joint R1 and subsequently the collapse of the entire bridge. It is important to note that the loss of a half-joint in load configurations L1 and L2, representative of design loads, does not result in a potential progressive collapse.

Finally, the quantification of robustness through appropriate indices, along with other indicators such as safety factors, cost, sustainability, etc., can guide designers in selecting the optimal retrofitting solution over other intervention options for existing bridges. Additionally, it can aid managing authorities in prioritizing maintenance and repair interventions for existing bridges.

## CRediT authorship contribution statement

**Paolo Martinelli:** Writing – review & editing, Writing – original draft, Validation, Methodology, Investigation, Formal analysis, Data curation, Conceptualization. **Matteo Colombo:** Writing – review & editing, Validation, Methodology, Investigation, Formal analysis, Conceptualization, Supervision. **Marco di Prisco:** Writing – review & editing, Validation, Supervision, Funding acquisition.

## Declaration of Competing Interest

The authors declare that they have no known competing financial interests or personal relationships that could have appeared to influence the work reported in this paper.

## Data Availability

Data will be made available on request.

## Acknowledgements

This work has been supported by the project "FIRMITAS: multi-hazard assessment, control and retroFIt of bridges for enhanced Robustness using sMart IndusTriAlized Solutions" funded by the Italian PRIN project 2020, grant n. 2020P5572N.

## References

[1] Anitori G, Casas JR, Ghosn M. Redundancy and robustness in the design and evaluation of bridges: European and North American Perspectives. J Bridg Eng 2013;18:1241–51. https://doi.org/10.1061/(asce)be.1943-5592.0000545.
[2] Au FTK, Leung CCY, Kwan AKH. Collapse mechanism and robustness of precast segmental bridges. Proc Inst Civ Eng Bridg Eng 2014;167:303–14. https://doi.org/10.1680/bren.11.00045.
[3] Bontempi F. Elementary concepts of structural robustness of bridges and viaducts. J Civ Struct Heal Monit 2019;9:703–17. https://doi.org/10.1007/s13349-019-00362-7.
[4] Fan BH, Su JZ, Chen BC. Condition evaluation for through and half-through arch bridges considering robustness of suspended deck systems. Adv Struct Eng 2021;24:962–76. https://doi.org/10.1177/1369433220945835.
[5] Cavaco ES, Casas JR, Neves LAC, Huespe AE. Robustness of corroded reinforced concrete structures - a structural performance approach. Struct Infrastruct Eng 2013;9:42–58. https://doi.org/10.1080/15732479.2010.515597.
[6] Cavaco ES, Neves LAC, Casas JR. On the robustness to corrosion in the life cycle assessment of an existing reinforced concrete bridge. Struct Infrastruct Eng 2018;14:137–50. https://doi.org/10.1080/15732479.2017.1333128.
[7] Ghosn M, Moses F, Frangopol DM. Redundancy and robustness of highway bridge superstructures and substructures. Struct Infrastruct Eng 2010;6:257–78. https://doi.org/10.1080/15732470802664498.
[8] Jiang R, Wu Q, Chen Y, Yi X, Tu J. About the structural robustness of through arch bridges. Appl Mech Mater 2012;178–181:2412–7. https://doi.org/10.4028/www.scientific.net/AMM.178-181.2412.
[9] Shoghijavan M, Starossek U. Structural robustness of long-span cable-supported bridges in a cable-loss scenario. J Bridg Eng 2018;23:04017133. https://doi.org/10.1061/(asce)be.1943-5592.0001186.
[10] Shoghijavan M, Starossek U. Developing a robustness index for parallel load-bearing systems. Eng Struct 2021;244:112742. https://doi.org/10.1016/j.engstruct.2021.112742.
[11] Wang M, Zhou Z. Progressive collapse and structural robustness of bridges. Appl Mech Mater 2012;193–194:1021–4. https://doi.org/10.4028/www.scientific.net/AMM.193-194.1021.
[12] Wisniewski D, Casas JR, Ghosn M. Load capacity evaluation of existing railway bridges based on robustness quantification. Struct Eng Int 2006;16:161–6. https://doi.org/10.2749/101686606777962440.
[13] Olmati P, Brando F, Gkoumas K. Robustness assessment of a steel truss bridge. Struct Congr 2013 Bridg Your Passion Your Prof - Proc 2013 Struct Congr 2013:250–61. https://doi.org/10.1061/9780784412848.023.
[14] Buitrago M, Bertolesi E, Calderón PA, Adam JM. Robustness of steel truss bridges: Laboratory testing of a full-scale 21-metre bridge span. Structures 2021;29:691–700. https://doi.org/10.1016/j.istruc.2020.12.005.
[15] Saracco U, Felitti M, Oliveto F, Alvaro MR, Formisano A. Robustness evaluation of a steel bridge in the district of Potenza (Italy). Procedia Struct Integr 2022;44:721–8. https://doi.org/10.1016/j.prostr.2023.01.094.
[16] Caredda G, Porcu MC, Buitrago M, Bertolesi E, Adam JM. Analysing local failure scenarios to assess the robustness of steel truss-type bridges. Eng Struct 2022;262:114341. https://doi.org/10.1016/j.engstruct.2022.114341.
[17] CNR. CNR DT 214/2018, Guide to Design of Structures for Robustness 2021.
[18] André J, Anghileri M, Belletti B, Biondini F, Caspeele R, Demonceau J-F,Izzuddin B, Martinelli P, Molkens T, O'Connor A, Parisi F, Sio J, Sousa ML,Thienpont T. JRC Technical Report - Guidance on the design for structuralrobustness. Joint Research Centre (JRC); 2024.
[19] Moreira V., Fernandes J., Matos J., Olivera D. Robustness as Performance Indicator for masonry arch bridges. COST Action TU1406 Eb. 1st Work. Meet. Geneva ETH-Zürich, 2016.
[20] Biondini F., Frangopol D. Life-cycle robustness of deteriorating concrete structures. Int. Conf. Performance-based Life-cycle Struct. Eng., Brisbane, QLD, Australia: 2015. doi:10.14264/uql.2016.547.
[21] Björnsson I, Thelandersson S. Robustness analysis of bridge when exposed to traincollision due to derailment. COST ACTION C26 Urban Habitat Constr Catastro Events 2010:603–8.
[22] Autostrade per L'Italia. Report di analisi delle principali tipologie strutturali di opere presenti sulla rete ASPI. (In Italian) 2022.
[23] MIMS (Ministero delle Infrastrutture e della Mobilità Sostenibile). Linee guida per la classificazione e gestione del rischio, la valutazione della sicurezza ed il monitoraggio dei ponti esistenti. (In Italian) 2022:90.
[24] Martinelli P, Colombo M, di Prisco M. Robustness of RC girder bridges: the case of half-joint bridges. In: Biondini F, Frangopol D, editors. Life-Cycle Struct. Infrastruct. Syst. Proc. eighth Int. Symp. life-cycle Civ. Eng. (IALCCE 2023). London: CRC Press, Taylor & Francis Group; 2023. p. 3856–63. https://doi.org/10.1201/9781003323020-473.
[25] di Prisco M, Colombo M, Martinelli P. Structural Aspects of the Collapse of a RC Half-Joint Bridge: Case of the Annone Overpass. J Bridg Eng 2023;28:05023007. https://doi.org/10.1061/jbenf2.beeng-6063.
[26] Adam JM, Parisi F, Sagaseta J, Lu X. Research and practice on progressive collapse and robustness of building structures in the 21st century. Eng Struct 2018;173:122–49. https://doi.org/10.1016/j.engstruct.2018.06.082.
[27] Starossek U. Measures of robustness and collapse resistance. Progress Collapse Struct 2017:129–40. https://doi.org/10.1680/pcos.61682.129.
[28] Biondini F, Restelli S. Damage propagation and structural robustness. Life-Cycle Civ Eng - Proc 1st Int Symp Life-Cycle Civ Eng IALCCE 2008;08:131–6. https://doi.org/10.1201/9780203885307.ch14.
[29] Starossek U. Typology of progressive collapse. Progress Collapse Struct 2017:18–42. https://doi.org/10.1680/pcos.61682.018.
[30] Biondini F, Frangopol DM, Restelli S. On structural robustness, redundancy and static indeterminacy. Proc 2008 Struct Congr - Struct Congr 2008 Crossing Bord 2008;314. https://doi.org/10.1061/41016(314)237.
[31] Frangopol DM, Curley J. Effects of damage and redundancy on structural reliability. J Struct Eng 1987;113:1533–49. https://doi.org/10.1061/(ASCE)0733-9445(1987)113:7(1533).
[32] Biondini F. A measure of lifetime structural robustness. Proc 2009 Struct Congr - Don't Mess Struct Eng Expand Our Role 2009:1749–57. https://doi.org/10.1061/41031(341)193.
[33] André J. Structural robustness: a revisit. Struct Eng Mech 2020;76:193–205. https://doi.org/10.12989/sem.2020.76.2.193.
[34] Circular 14 February 1962 No. 384 - Norme relative ai carichi per il calcolo dei ponti stradali. (In Italian) 1962.
[35] di Prisco M., Colombo M., Martinelli P., Coronelli D. The technical causes of the collapse of Annone overpass on SS.36. In: di Prisco M., Menegotto M., editors. Ital. Concr. Days 2018, Associazione Italiana Calcestruzzo Armato e Precompresso (AICAP) / Collegio dei Tecnici della Industrializzazione Edilizia (CTE); 2018, p. 16.

[36] NTC 2018. Aggiornamento delle norme tecniche per le costruzioni. Decreto del Ministro delle Infrastrutture del 17 gennaio 2018. Gazzetta Ufficiale Serie Generale n. 42 del 20–02–2018 (In Italian) 2018.
[37] Dassault Systèmes. Abaqus Analysis User's Manual - Version 2021 2021.
[38] fib (Fédération internationale du béton). fib Model Code for Concrete Structures 2010. Lausanne; 2013.
[39] fib (Fédération internationale du béton). fib Bulletin 63. Design of precast concrete structures against accidental actions Lausanne 2012.
[40] fib (Fédération internationale du béton). fib Model Code 2020 - Draft Sub Chapter 30.9 (Design for robustness) 2022.
[41] Rodríguez D, Brunesi E, Nascimbene R. Fragility and sensitivity analysis of steel frames with bolted-angle connections under progressive collapse. Eng Struct 2021; 228:111508. https://doi.org/10.1016/j.engstruct.2020.111508.
[42] Martinelli P, Colombo M, Ravasini S, Belletti B. Application of an analytical method for the design for robustness of RC flat slab buildings. Eng Struct 2022;258: 114117. https://doi.org/10.1016/j.engstruct.2022.114117.
[43] Mpidi Bita H, Tannert T. Disproportionate collapse prevention analysis for post and beam mass timber building. J Build Eng 2022;56:104744. https://doi.org/10.1016/j.jobe.2022.104744.